



Assessment of plastic zones surrounding the power station cavern using numerical, fuzzy and statistical models

Mohammad Rezaei¹ · Morteza Rajabi²

Received: 10 October 2019 / Accepted: 7 December 2019 / Published online: 18 December 2019
© Springer-Verlag London Ltd., part of Springer Nature 2019

Abstract

Plastic zones evaluation around the powerhouse caverns is a very crucial issue in designing and constructing these structures and accurate determination of their related optimum support systems. Due to inherent difficulties during the field measurement of plastic zones around the powerhouse caverns and shortcomings of the available methods in this field, applying new predictive models is an attractive and helpful topic. Accordingly, plastic zones around the powerhouse caverns have been investigated in this research using numerical analysis (NA), fuzzy inference system (FIS) and multivariate regression (MVR) model. Based on the numerical simulations, a new predictive equation has been developed to determine the plastic zone at middle point of sidewall and induced key point around a cavern. The basic parameters including rock geomechanical properties and geometrical characteristics of cavern structures have been considered as input variables in plastic zones modeling at middle points of roof, floor, left sidewall and right sidewall as well as at key point. For FIS and MVR models construction, sufficient datasets were introduced based on the numerical simulations. Performance of established models has been assessed applying testing dataset and utilizing powerful statistical indices. Accordingly, it is proved that the derived results from FIS and NA models are more precise than MVR model and they are more satisfactory in plastic zone estimation. Finally, parametric study results revealed that lateral stress coefficient, depth of overburden and rock mass rating are the most effectual parameters and tensile strength is the least influencing parameter on the plastic zone around a cavern.

Keywords Power station cavern · Plastic zone · Numerical analysis · Fuzzy inference system · Multivariate regression

1 Introduction

During and after the excavation of underground spaces inside the weak rocks located at the high depth, there exists the high ratio of in situ horizontal stress to vertical stress. In this situation, the high extension of plastic zone (PZ) will be induced in the rock mass around these spaces. This condition may occur when the induced stresses in the surrounding rock masses exceed the yield stress or rock mass strength.

Extension of PZ depends on the rock mass characteristics, geometry or shape of the opening and its excavation method. On the other hand, the size and shape of PZ are the critical variables to analyze the stability of underground spaces and quantitative design of their related support requirements. There are various methods for prediction of PZ around the underground spaces such as theoretical and numerical models. Accordingly, different investigations were performed to study PZ around the underground spaces using the above-mentioned methods.

Zhu et al. [1] studied the displacement at the high wall of a series of underground caverns based on the numerical simulations with multiple schemes. They concluded that the best relations to estimate the displacement at the side wall key points were achieved using the dimensionless approach. Chong et al. [2] analyzed the distribution of PZ in the rock mass surrounding the rectangular gates using FLAC^{3D} software and considering the different spans and coefficients lateral pressure. Applying the FLAC^{3D} software, Feng et al. [3] estimated the value of plastic

Electronic supplementary material The online version of this article (<https://doi.org/10.1007/s00366-019-00900-3>) contains supplementary material, which is available to authorized users.

✉ Mohammad Rezaei
m.rezaei@uok.ac.ir

¹ Department of Mining Engineering, Faculty of Engineering, University of Kurdistan, Sanandaj, Iran

² Department of Mining Engineering, Shahid Bahonar University of Kerman, Kerman, Iran

deformation in hard and soft rock zones surrounding a tunnel. Xiang and Feng [4] presented a theoretical procedure to predict the potential PZ around the shallow tunnel in the neighborhood of pile foundation. Zhang and Goh [5] proposed a new non-parametric regression model to study the influence of geotechnical and geomechanical parameters on the strain and maximum displacement at the key point. Chen et al. [6] predicted the depth of PZ at the upstream and downstream sidewalls of powerhouse caverns using numerical simulation. Yu et al. [7] analyzed the rock fracture and stability of rock mass around the underground caverns using the numerical method. On the basis of the numerical simulations, Zhang and Goh [8] developed some statistical regression models to estimate the safety factor and maximum displacement around the multiple caverns. Zhang et al. [9] applied the in situ monitoring techniques to measure the displacement of a group of underground caverns and verified them using the 3D numerical model. On the basis of the monitoring measurements, Li et al. [10] showed that the fractures and deformations around the underground caverns are increased by increasing the excavation steps. Jiang et al. [11] showed that the results of their developed numerical model were completely in accordance with the measured deformations around the large underground caverns. The applicability of the statistical approach to assess the deformability of rock mass surrounding the powerhouse cavern under different conditions was demonstrated by Behnia and Cheraghi Seifabad [12]. A back-analysis approach was developed by Gao et al. [13] to estimate the PZ distribution and displacement prediction around the caverns which was verified by the numerical experiments. They achieved the reliable results which are practically similar to the field measurements. Li et al. [14] studied the rupturing fracture of rock mass around the underground caverns based on the principle of energy dissipation and verified their findings by the numerical modeling results. Xua et al. [15] presented an analytical approach to find the PZ distribution surrounding the openings and verified its results with the results of the FLAC^{2D} numerical model. Based on this approach, they evaluated the effect of lateral pressure coefficients and slot depths variations on the PZ extension. Moreover, failure mechanism and deformation prediction at different locations of rock mass neighboring the underground powerhouse was studied by Wang et al. [16] for safely construction goals. Deformation estimation and safety analysis of rock surrounding a cavern was conducted by Ren et al. [17] to select the optimum supports and provide the required safety during the cavern construction. Finally, Li et al. [18] presented a numeric-microseismic model to assess the deformation of rock mass surrounding underground caverns. They proved that prediction of rock mass

displacements based on the numeric-microseismic model can give the better estimations for real in situ conditions.

Considering the nature of understudied problem, it is relatively difficult to predict PZs surrounding the powerhouse station cavern which can be evidently observed in the above studies. Indeed, previous studies were focused on the PZ evaluation around the single tunnels and there are a few numbers of researches that focused on the prediction/estimation of PZs surrounding the powerhouse caverns. This is due to the fact that the powerhouse environment is a complex space in which the several adjacent openings have interacted together. On the other hand, the majority of the previous utilized methods are the numerical approaches that just can be applied for the particular case studies. Therefore, these specific developed numerical models cannot be effectively applied for other cases/lotions. Moreover, unknown relationships and inherent interactions between the many effective parameters and PZ around the power station caverns may not be completely appropriate for theoretical and numerical modeling due to the problem nature [4]. Bearing in mind the above-mentioned weakness of current theoretical and numerical approaches, utilizing the new predictive intelligent models, i.e., fuzzy inference system (FSI) might duly cover the shortcomings in the estimation of PZ surrounding the powerhouses. In the recent years, FSI and some of the other intelligent approaches were employed as the most efficient predictive tools to investigate the rock engineering and geomechanics problems related to the surface and underground structures [19–30]. Some authors have also utilized the theory of fuzzy mathematics to analyze the rock mass displacement and deformation as a result of underground excavations [31–33]. Certainly, FIS model can cover the above restrictions and provide the possible requirements in the estimation of plastic zones around the power station caverns. Despite these applications, FIS approach was not applied in the field of PZs prediction around the powerhouse station until now as it is observed from the comprehensive literatures review. Therefore, examining the FIS application in this field can be an attractive topic and used as a worldwide approach which may present the desired results compared to the previous ones.

In addition to the above-referred shortcomings of existing methods, the PZ at the roof, floor, sidewalls and key points were not simultaneously studied in a comprehensive research until now. Meanwhile, the extent of plastic zones surrounding the power station caverns including the middle points of roof, floor, left sidewall and right sidewall as well as the key points (maximum plastic zone) have been simultaneously investigated in this research. Moreover, all of the possible effective geomechanical and geometrical parameters were considered in the estimation of the PZs at different points around the power station caverns unlike the previous researches. This can help the comprehensive, ideal

and efficient estimation of support requirements for the powerhouse caverns and the multiple opening in tunneling and underground spaces constructions. For this purpose, new empirical equations were firstly developed in this research based on the extensive numerical analysis. Secondly, a new fuzzy inference system was constructed to predict PZs surrounding the powerhouse caverns for covering the aforementioned requirements in the field of PZ estimation and establishment of a worldwide model. Finally, comparison analysis was made between the findings of the numerical analysis, fuzzy inference system and multivariate regression model.

2 Applied methods

In this research, three models including numerical analysis (NA), fuzzy inference system (FIS) and conventional multivariate regression (MVR) analysis were utilized to estimate the complete PZs around the power station caverns. The basic descriptions of these approaches will be briefly overviewed in the following sub-sections.

2.1 Numerical analysis

With advances in computer systems, various numerical-based software programs have been effectively developed for practical application in different engineering fields. Numerical modeling was extensively utilized in different sciences/industries to solve the existing problems. In the fields of geotechnics and rock mechanics, numerical modeling can help the engineers to design the underground excavations and related support systems. These models were also applied to conduct the parametric studies, provide the possible range of the system responses and consider the possible influencing variables involved in the modeling. These lead to understand the key variables in the modeling which can help set priorities for further site investigation and material testing to introduce suitable data utilized in designing phases. There are several numerical methods used in solving the different engineering problems. These methods were categorized as finite element method (FEM), discrete (distinct) element method (DEM), boundary element method (BEM), material point method (MPM), finite difference method (FDM), etc. Among them, DEM is considered as the discontinuum method; whereas, FDM, BEM and FEM types belong to the continuum methods. However, none of these methods is proved as an optimum method for all engineering problems. Each of them has some advantages/limitations for the specific problems [34]. Due to the capabilities of FEM in the modeling of rock mechanics problems and the simplicity of its coding programs, this program was used to conduct the numerical analysis in this study.

2.2 Fuzzy inference system

The idea of ‘‘fuzzy set’’ was firstly introduced as the ‘‘fuzzy set theory’’ by Zadeh [35]. The comprehensive review on the basis of this theory and construction of the fuzzy models were previously performed by different investigators [19–26]. Therefore, fuzzy set theory, fuzzy inference systems (FISs) and fuzzy modeling steps are briefly outlined in this section. It is obvious that the value of membership of each element in a classical (crisp) set is equal to 1 if it belongs to a set and equal to 0 if it does not belong to a set. On the contrary, the elements in a fuzzy set can take the membership values in the range of 0–1. Construction of a FIS is generally composed of four fundamental stages including input numeric values fuzzification, development of fuzzy rules (construction of fuzzy rule base), selection of fuzzy interference engine and defuzzification of fuzzy output values.

In the first stage, suitable membership functions (MFs) have been developed to convert the numeric input values into the fuzzy linguistic expressions. The MFs are also applied to map and transfer the input vectors into the fuzzy ‘‘if–then’’ rules inside the rule base. There exist different forms of MFs, i.e., linear shape including triangular and trapezoidal shape and non-linear shape including Gaussian, Z and S types. The utilization of these MFs depends on the nature of understudied problem. In the next stage, the relationships of input–output variables are described by fuzzy rules in the ‘‘if–then’’ forms to construct the ‘‘rule base’’.

In the third stage, an appropriate inference engine is generally determined to combine the fuzzy ‘‘if–then’’ rules for obtaining the fuzzy outputs on the basis of the fuzzy composition rules. Different types of FIS including Takagi–Sugeno–Kang (TSK), Mamdani, Tsukamoto and Singleton engines exist that can be applied to solve the problems related to the science, engineering and technology fields. In this paper, the algorithm of Mamdani was applied because it is simpler and efficient to construct and examine in geosciences modeling compared to the other types [19]. This algorithm is one of the first developed fuzzy set theories that worked on the basis of the control systems. Mamdani algorithm was firstly introduced by Mamdani and Assilian [36] in 1975. There exist many aggregation methods that are used to combine the fuzzy rules in the Mamdani algorithm. These methods include min–max, max–max, min–min and max–min types. Among them, max–min composition was a commonly applied method [19]. Conversion process of the fuzzy outputs to the crisp (numeric) ones is the last step of FIS modeling which was named the defuzzification process. There exist various defuzzification approaches including center of gravity (COG), mean of the maximums (MOM), smallest of the maximums (SOM) and centroid of area

(COA). However, it was proved that the most commonly utilized approach is the COA [19].

2.3 Multivariate regression analysis

Conventional multivariate regression (MVR) analysis is one of the statistical regression divisions that is utilized in the modeling of science and engineering problems. The aim of the regression modeling is the construction of an approximate model that can correlate the input parameter(s) with the output (objective) parameter(s) to achieve the minimum possible error [37]. In statistics science, MVR is the efficient technique to represent the correlation between an output parameter and a series of input parameters. In the MVR analysis, data are analyzed utilizing the linear relations/functions and then, the indefinite parameters of the model can be predicted/estimated from the data.

3 Numerical analysis of PZ

In the numerical analysis (NA) of the current study, 2D finite element program was applied to estimate PZs in the excavation boundary around a powerhouse cavern. For this purpose, four fundamental assumptions have been made as follows:

- The masses around the powerhouse are isotropic, homogeneous and quasi continuous.
- In the horizontal and vertical directions, there are two main stresses (major and minor).
- Two types of powerhouse are considered in the modeling (a house horse-shoe shape cavern having the cross section with 33×52 m dimension and a transformer cavern having the cross section with 13×19 m dimension).
- A model with plane strain hypothesis was used in the modeling for the cases that the cavern was too lengthy.

Table 1 shows the interval of considered effective variables as the inputs of numerical analysis including the geometrical and geomechanical properties of rocks surrounding the excavated cavern. Additional required rock

mass characteristics for modeling were obtained utilizing the RocLab simulation program [38]. For this purpose, the ground was assumed as the elasto-plastic environment acted under the criterion suggested by Mohr and Coulomb. Moreover, the factor of expansion equal to 5 with “Box Boundary Type” and factor of gradation equal to 0.1 with “Graded Mesh Type” were considered in all of the conducted numerical models. Therefore, the outside dimensions of the models can be equal to the five times of the caverns width. The above-mentioned boundary conditions lead to fixed condition of X in left and right boundaries and fixed condition of Y in upper and lower boundaries of the constructed model. After the model geometry stabilization, meshing process can carry out automatically or manually. Here, the automatic procedure was utilized, while rock masses surrounding the caverns have the same characteristics. On the contrary, the manually mode was applied for mesh generation since the rock mass surrounding the caverns is assumed as semi-continuous environment. As the mesh generation was completed, all of the nodes upon the external side of boundary were situated in a fixed boundary condition without any displacement. Figure 1 indicates the schematic representation the geometry of the powerhouse and transformer along with their boundary conditions. Moreover, NA model geometric layout, steps of excavation (ES_i) and the state of the key points in examinations are demonstrated in Fig. 2. In general, Fig. 2 is the graphical representation of a powerhouse cavern in which the key points at the two lateral sidewalls and floor are marked. In Fig. 2, B and Z are the spacing and vertical distance of two neighboring caverns, respectively. This means that the maximum PZ is sometimes created in the floor of the powerhouse but in most cases the maximum PZ occurred in the powerhouse sidewalls which is greater than those of floor or roof. The further descriptions of this issue will be outlined in the next section.

3.1 Maximum depth of PZ around the powerhouse cavern

The maximum plastic zone was firstly investigated by Zhu et al. [40]. They characterized that the maximum plastic zone (MPZ) at the sidewall key point of powerhouse is somewhat more than the other powerhouse that surrounds.

Table 1 Intervals of geometrical and geomechanical properties of rocks surrounding the excavated caverns in the NA modeling (after Rajabi et al. [39])

| RMR | C (MPa) | φ (deg) | σ_t (MPa) | σ_c (MPa) | ν (-) | E (MPa) | K | H_0 (m) | B (m) | Z (m) |
|-----|-----------|-----------------|------------------|------------------|-----------|-----------|-----|-----------|---------|---------|
| 47 | 1.47 | 44.16 | 0.04 | 13.48 | 0.27 | 4350 | 0.7 | 100 | 20 | - 10 |
| 54 | 1.6 | 54.62 | 0.145 | 25.908 | 0.27 | 11,900 | 1 | 200 | 30 | 0 |
| 67 | 3.093 | 51.34 | 0.715 | 29.978 | 0.25 | 29,000 | 1.5 | 300 | 40 | 10 |
| 78 | 4.976 | 56.94 | 1.567 | 54.154 | 0.25 | 40,973 | 2 | 400 | 50 | 20 |
| | | | | | | | 2.5 | 500 | | |
| | | | | | | | | 600 | | |

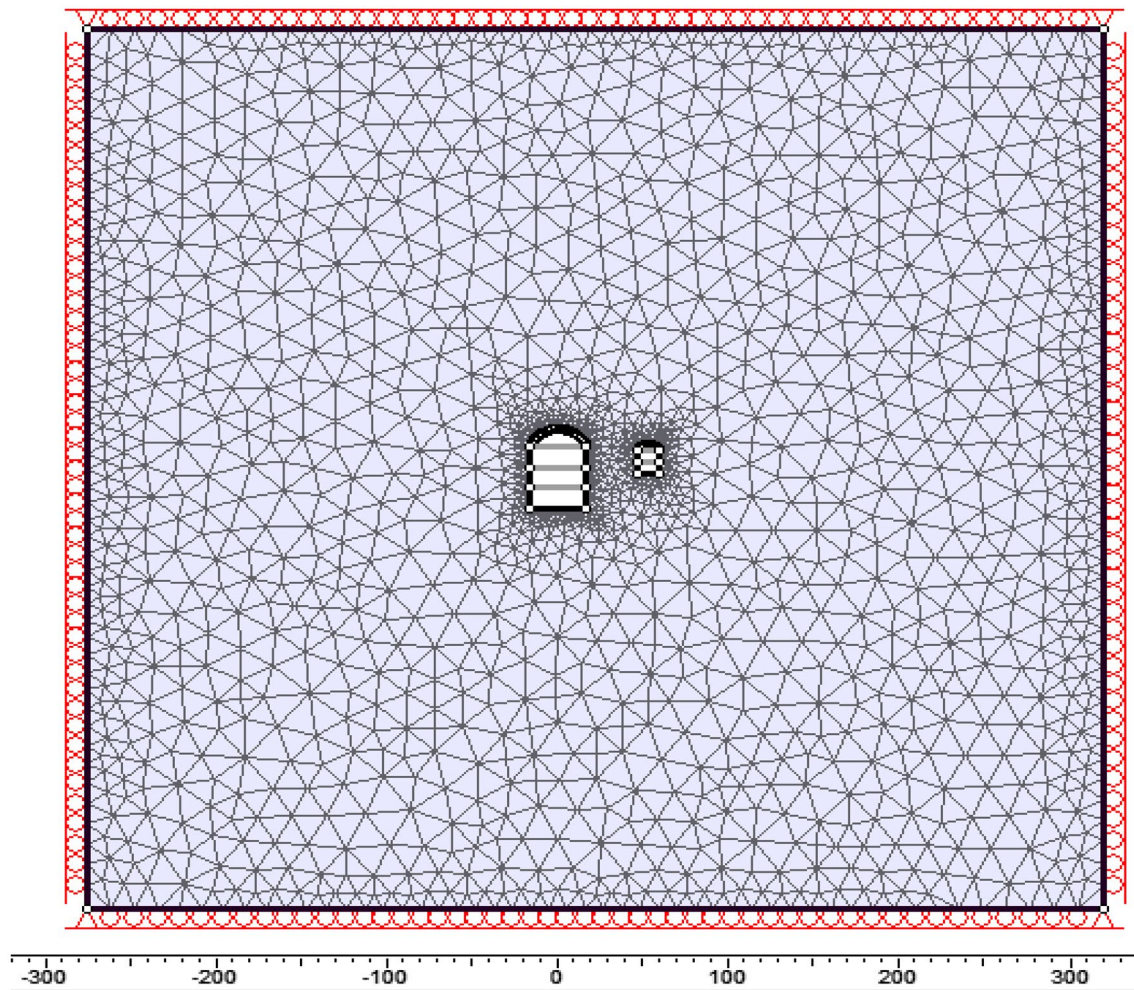


Fig. 1 The schematic representation of a powerhouse and transformer geometry and their boundary conditions in the NA modeling [39]

Besides, Abdollahipour and Rahmannedjad [41] proved that the MPZ in the sidewall is higher than the roof. To investigate maximum depth of the plastic zone (MDPZ) around the powerhouse cavern in this research, different conditions under Mohr–Coulomb failure criterion were considered in PZ as shown in Table 1. In addition, the depth of PZ was considered in the calculations, while more than 50% of the blocks have the plastic failure conditions. Based on the above-mentioned conditions, numerous numerical analyses were conducted. The obtained results are given in Figs. 3 and 4. As shown in Fig. 3a, in weak and medium rocks ($RMR=47$) with horizontal distance, i.e., 30, 40 and 50 m and low values of lateral pressure coefficients including $k=0.7$ or $k=1$, the MDPZ occurs on the left sidewall in most cases and sometimes on the right sidewall. However, under those conditions but with $k=1.5$, the MDPZ forms on the powerhouse floor in most cases and sometimes on the sidewalls as demonstrated in Fig. 3b. For $k=2$, MDPZ frequently occurs on the right sidewall and sometimes in the

floor or the left sidewall of powerhouse which is represented in Fig. 3d. Finally, for $k=2.5$, MDPZ is located on the right sidewall in more cases and on the left sidewall of powerhouse cavern in less cases which is displayed in Fig. 3c. On the other hand, for $RMR=67$ and $k=1.5–2$, MDPZ is located on the powerhouse floor in all cases; whereas for $k=2.5$, MDPZ is located on the right sidewall in more cases and sometimes occurs on the left sidewall of powerhouse as depicted in Fig. 4a, b. Also for $RMR=78$, the key point is always located on the right sidewall of powerhouse when $H \leq 300$ m and $k=2.5$. Contrariwise for $H \geq 300$ m and $k=2.5$, MDPZ is positioned on the floor in more cases and on the right sidewall of powerhouse in some cases. Eventually, the key point or MDPZ continuously occurs on the floor when $H \geq 300$ m and $k=2$. The later conditions are demonstrated in Fig. 4c, d.

As it can be seen from Figs. 3 and 4, the key point location is varied on the powerhouse sidewalls or floor of the powerhouse. Therefore, it is better to consider the key zone in the

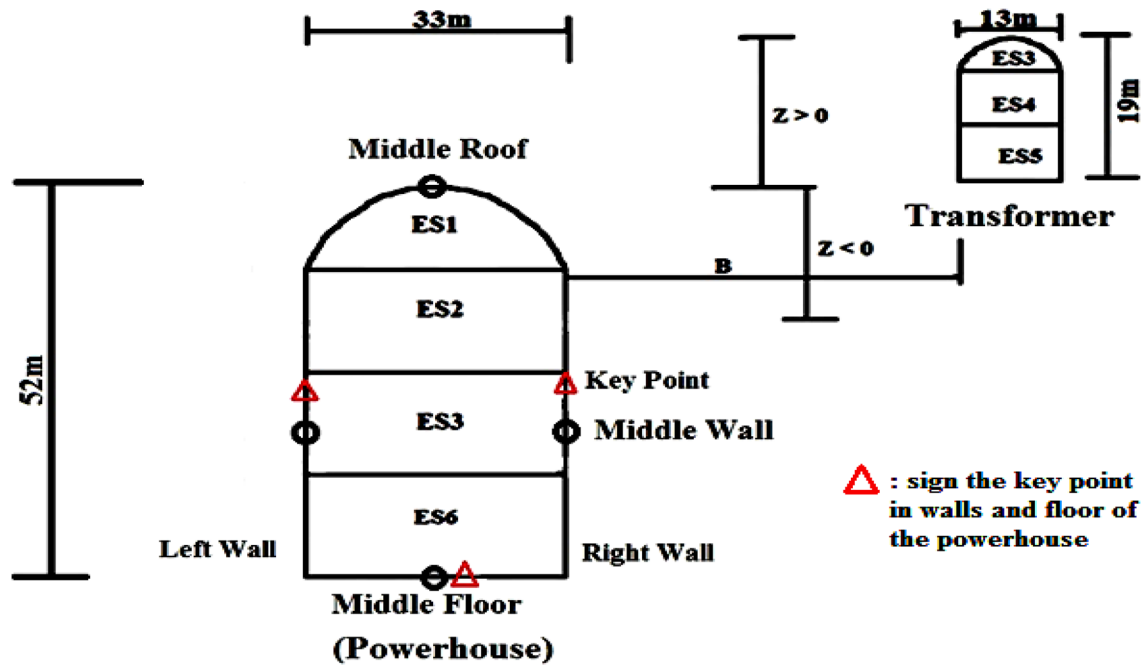


Fig. 2 NA model geometric layout, steps of excavation (ESi) and the state of key points (after Rajabi et al. [39])

floor or lateral sidewalls of a powerhouse. On the other word, this key point was located at the top sidewall in some cases ($RMR = 47, 54, K = 2$ or 2.5 and Z i.e. $+10, +20$ meters) as shown in Figs. 3e, f and 4b. Moreover, in the case of $K = 1.5$, key point is located at the powerhouse floor. According to the above investigations, it is concluded that this key point was frequently situated on the powerhouse sidewalls.

4 Numerical formula to predict PZ

Due to the effect of transformer cavern on the right sidewall of main cavern, PZ prediction in this area is conducted using the numerical method (NM) in the current section. To predict PZ at the powerhouse right sidewall (RS_p), key point (MPZ) and middle point, numerous numerical analyses (about 1920 series) were conducted under various conditions presented in Table 1. Various curve series (about 768 series) were achieved from the numerical experiments to show the variations of relative PZs (Pz/h) at the right sidewall key points and middle point of powerhouse against the relative lateral loading ($1000k\gamma H/E$) for some rock types based on the RMR rating system (Fig. 5). Therefore, the following equation was developed for prediction of PZ at the determined points of the powerhouse:

$$PZ = h[a(1000k\gamma H/E)^2 + b(1000k\gamma H/E) + c(B/H) + d(Z/H) + e] \quad (1)$$

where Pz is plastic zone depth at the powerhouse right sidewall key points and middle point (m), γ is unit weight of

rock (N/m^3), h is powerhouse height, k is coefficient of lateral pressure, E is deformation modulus of rock mass (Pa), H is overburden depth (m) that computed from the ground surface to the powerhouse floor ($H = H_0 + h$), B is width of pillar (m), Z is difference of crown level (m) and; a, b, c, d and e constants are regression coefficients related to the depth of overburden and types of rock mass surrounding the cavern (see Tables 2 and 3).

It is observed from Fig. 5 that PZ in the surrounding rock is almost equal to zero for the good rock quality ($RMR = 78$) or low overburden depth values ($H_0 \leq 300$) with the lateral pressure coefficient less than 2. Also, Table 2 and 3 indicate that the c, d and e constants are very low and can be neglected for good rock quality ($RMR = 78$) and low overburden depth (i.e., $H_0 = 100$). On the contrary, for high overburden depth and poor rock quality, these coefficients cannot be ignored and the resulted relationship is not linear. In this situation, PZ will gradually occur at the sidewall (Fig. 4) and hence a parabolic shape of PZ would be created (Fig. 5).

Using Eq. (1) and the coefficients given in Tables 2 and 3, PZs were calculated for the middle point at the right sidewall and key points around the powerhouse. It should be noted that there exist no publications in the fields of in situ measurements regarding the complete plastic zones surrounding the powerhouse caverns in literatures. Thus, the achieved results from the current analyses were compared with the corresponding plastic zones obtained from

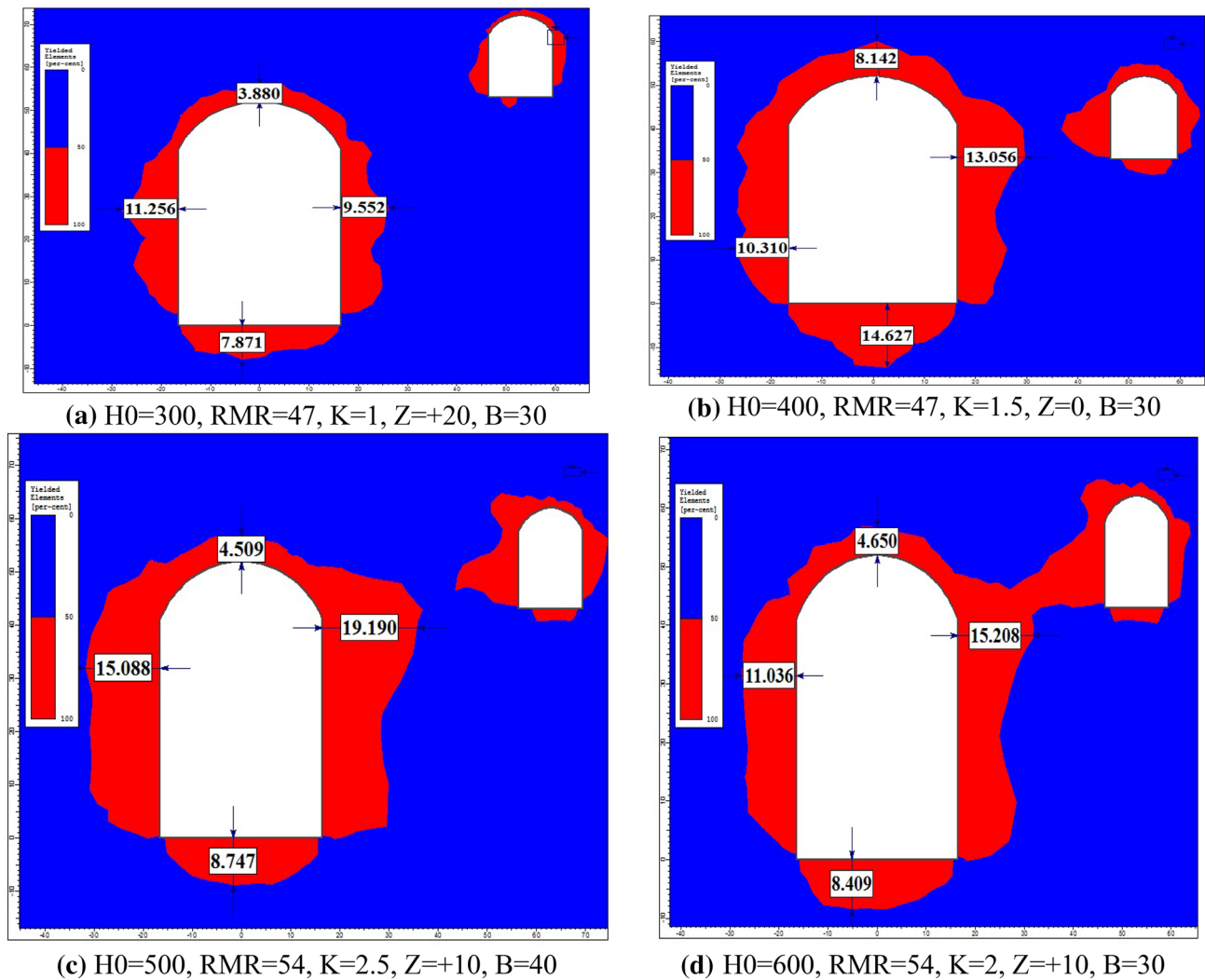


Fig. 3 Occurrence of MPZ at different locations: **a** left sidewall of powerhouse; **b** powerhouse floor; **c** and **d** powerhouse right sidewall ($RMR=47$ and 54)

the numerical program. The comparison results are demonstrated in Table 4. As it is observed from this Table, the resulted errors in the most examples are less than 13%. Therefore, it is concluded that the proposed equation in this research can be reliably applied in the most geomechanical conditions especially for the powerhouses with cross-section dimension of 33×52 m.

5 Database

In artificial intelligence modeling, sufficient numbers of datasets are necessary. In other words, collection of suitable data series is the main crucial step in the processing of these models. However, the numbers of input–output datasets depend on the geometry of the understudied

problem. Considering the complexity of practical measurement of occurred PZs in the powerhouse caverns environment, utilization of the numerical modeling results can be a useful database for this purpose. Accordingly, results of the conducted numerical analysis in the previous section were used to create a suitable database for designing and evaluating the new FIS and MVR models in this research. Based on the great number of numerical analysis calculations (1920 series), the twelve effective variables were regarded as input variables for PZs prediction at five main points surrounding the powerhouse caverns in FIS and MVR techniques. Descriptions of modeling parameters and their related signs and statistics are represented in Table 5. Moreover, Table 6 indicates some samples of datasets utilized in construction of FIS and MVR models.

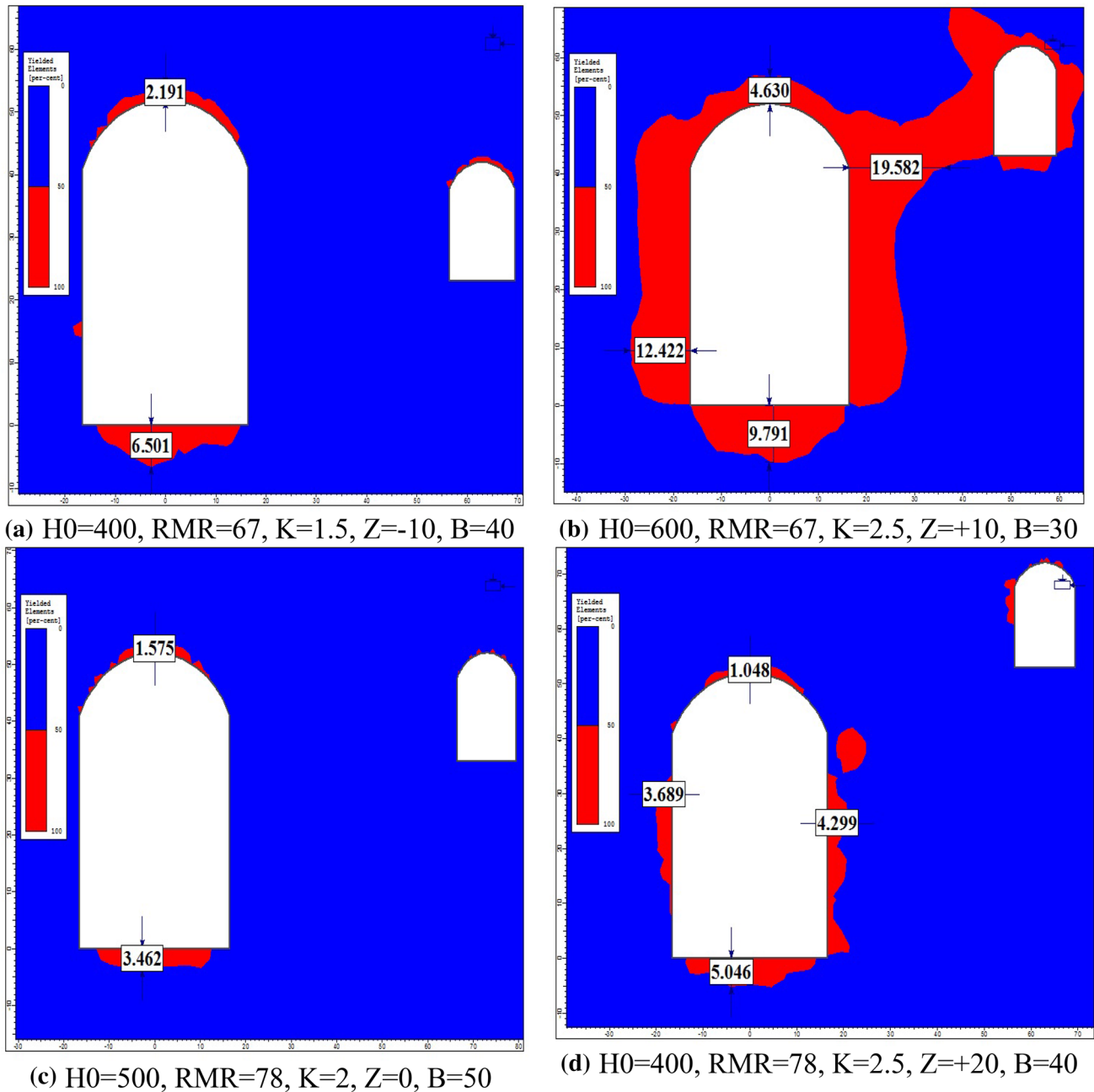


Fig. 4 Occurrence of MPZ at different locations: **a** powerhouse floor; **b** powerhouse right sidewall; **c** powerhouse floor ($RMR = 67$) and **d** powerhouse floor ($RMR = 78$)

6 Design of FIS model to determine PZs

In addition to the numerical analysis, a novel FIS model has been developed here in order to assess the PZs around the power station caverns. For determining PZs at five points around the power station cavern, twelve input parameters including tensile strength, rock mass modulus, unit weight of rock, lateral stress coefficient, Poisson ratio, compression strength, rock mass rating, friction angle, cohesion,

overburden depth, crown level difference and pillar width were utilized.

After the definition of fuzzy model structure, the first step of FIS modeling, i.e., inputs and outputs fuzzification was performed with the help of membership functions (MFs). The Gaussian membership function type was selected as the optimum membership function on the basis of the trial and error (TAE) procedure. To do that, FIS models with different types of MFs were examined based on the least amount

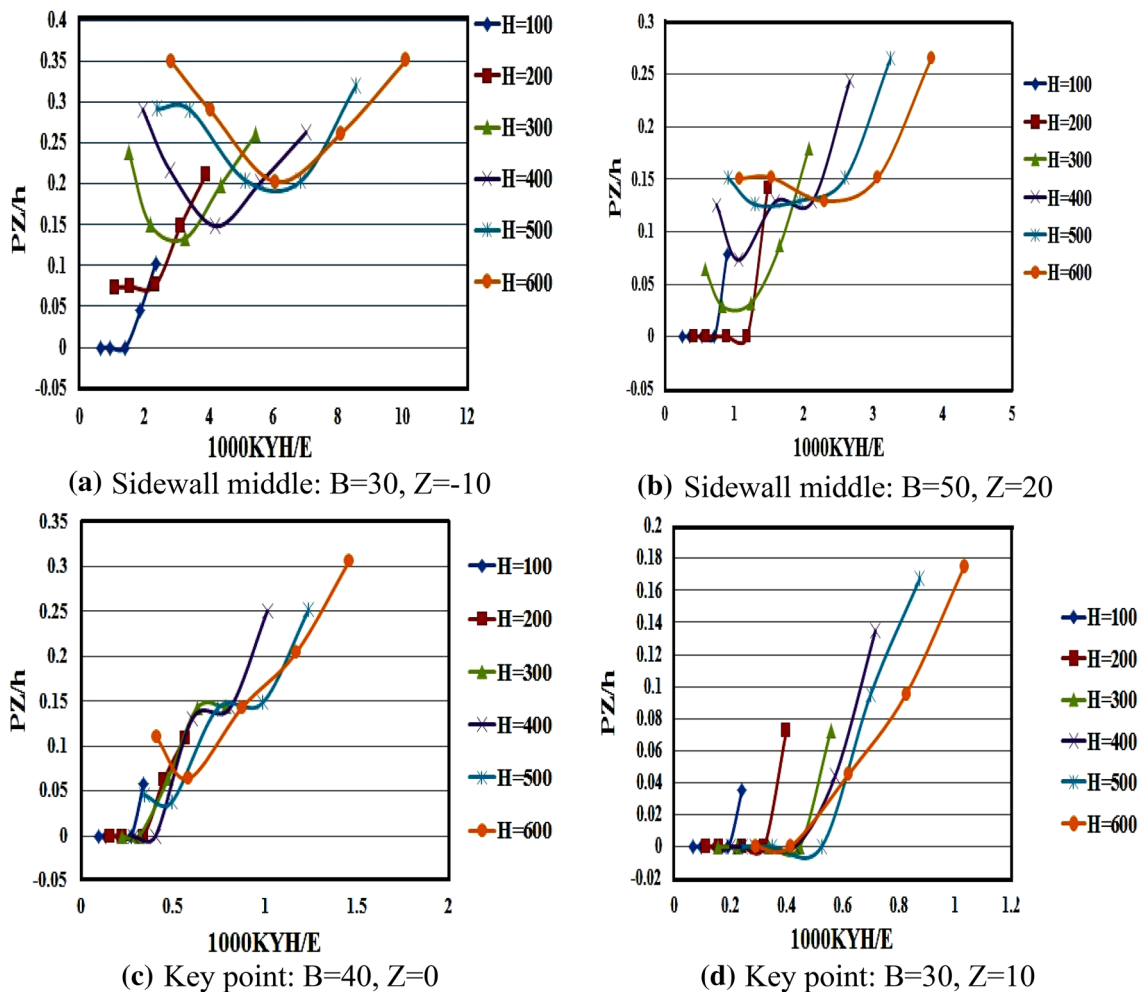


Fig. 5 Relation of PZs at right sidewall middle point and key points against the lateral loading considering different depths of overburden and for: **a** B=30, Z=- 10 m and RMR=47 **b** B=50 m, Z=+ 20 m

and RMR=54 **c** B=40 m, Z=0 m and RMR=67 **d** B=30 m, Z= 10 m and RMR= 78

of error value. Accordingly, the MFIS model with Gaussian membership function concluded the minimum value of the possible error and thus it was selected as the best one. As a result, this MF type was applied to fuzzify the input/output variables of the suggested FIS model in this research. In these MFs, the fuzzy sets were categorized into three main classification, i.e., ‘Low’, ‘Medium’ and ‘High’ classes.

The next step of FIS modeling is the construction of the powerful ‘rule base’ including suitable and adequate fuzzy ‘if-then’ rules in order to map the relationships between the input(s) and output(s). Discussed datasets in Sect. 4 along with the expert knowledge were utilized to conduct these rules and construct the fuzzy ‘rule base’. Accordingly, a total of 950 rules were developed for solving the understudied problem in this research. After the ‘rule base’ construction, fuzzy decision-making should be performed by using an appropriate engine or algorithm. This step is used to merge the premise part (input) and consequent part

(output) of fuzzy ‘if-then’ rules to map the fuzzy results of the model. Here, a Mamdani algorithm (engine) was applied to compute the fuzzy outputs. As the result of aggregation process (third stage of FIS modeling) is commonly a linguistic (fuzzy) value, it should be converted into a numeric/crisp value. This is the main object of forth step in fuzzy modeling which named the defuzzification process. In this step, TAE approach was also used to find the best one among the available defuzzification methods. According to this, COA defuzzification approach was selected as the best/optimum defuzzification method to obtain the numeric output values of the FIS model. Now, the suggested FIS model is ready to provide the precise estimation of PZs around the power station cavern by interring the suitable input variables values to it. A schematic representation of FIS decision-making and aggregation development of PZs prediction for a specific example in MATLAB package environment is demonstrated in Fig. 6. In this figure, input/output variables are

Table 2 Coefficient values of Eq. (1) to predict relative PZ at the key point

| | <i>RMR</i> | H_0 | <i>a</i> | <i>b</i> | <i>c</i> | <i>d</i> | <i>e</i> |
|--|------------|-------|----------|------------|-----------|-----------|-----------|
| | 47 | 100 | 0.041366 | 0.043387 | -0.159169 | 0.030236 | -0.016299 |
| | 54 | | 0.836831 | -0.638603 | -0.099633 | 0.051255 | 0.136120 |
| | 67 | | 2.455375 | -0.857741 | 0.001279 | 0.024825 | 0.063936 |
| | 78 | | 1.958687 | -0.484288 | -0.017919 | 0.004804 | 0.030568 |
| | 47 | 200 | 0.039610 | -0.092172 | -0.595714 | -0.046541 | 0.263486 |
| | 54 | | 0.150159 | -0.038376 | -0.320743 | 0.092187 | 0.035000 |
| | 67 | | 0.951480 | -0.377009 | -0.053138 | 0.065610 | 0.041232 |
| | 78 | | 1.435597 | -0.588475 | -0.020729 | 0.059937 | 0.054501 |
| | 47 | 300 | 0.029445 | -0.140726 | -0.675875 | -0.313890 | 0.449051 |
| | 54 | | 0.134040 | -0.213643 | -0.454062 | 0.051725 | 0.223120 |
| | 67 | | 0.052311 | 0.266304 | -0.101842 | 0.057575 | -0.061343 |
| | 78 | | 0.955969 | -0.547370 | 0.006667 | 0.041301 | 0.066737 |
| | 47 | 400 | 0.018150 | -0.113076 | -0.959509 | -0.254081 | 0.508593 |
| | 54 | | 0.092761 | -0.222741 | -0.624348 | 0.186727 | 0.317828 |
| | 67 | | 0.273676 | 0.033691 | -0.705369 | 0.085057 | 0.022706 |
| | 78 | | 0.537606 | -0.308223 | -0.097810 | 0.053568 | 0.048826 |
| | 47 | 500 | 0.013433 | -0.111904 | -1.066896 | -0.352465 | 0.594828 |
| | 54 | | 0.080530 | -0.2594650 | -1.245527 | -0.157829 | 0.450324 |
| | 67 | | 0.249867 | -0.114136 | -0.723279 | 0.362543 | 0.105378 |
| | 78 | | 0.431359 | -0.258612 | -0.287305 | 0.013892 | 0.055851 |
| | 47 | 600 | 0.007589 | -0.069937 | -2.461807 | -1.512148 | 0.658181 |
| | 54 | | 0.057590 | -0.219255 | -1.339112 | -0.147163 | 0.458296 |
| | 67 | | 0.247466 | -0.250343 | -0.959912 | 0.476535 | 0.219501 |
| | 78 | | 0.195430 | -0.031376 | -0.241608 | 0.160750 | 0.001676 |

demonstrated in format of numbers in which inputs ranged from 1 to 12 and outputs ranged from 1 to 5 according to Table 5 from up to down. As can be seen from this figure, in the case that the input variable values including unit weight = 0.027 KN/m³, tensile strength = 0.04 MPa, Poisson ratio = 0.27, coefficient of lateral stress = 0.7, compression strength = 13.5 MPa, rock mass modulus = 4.35 GPa, friction angle = 44.2°, cohesion = 1.47 MPa, overburden depth = 452 m, rock mass rating = 47, pillar width = 20 m and crown level difference = 0 have been entered to the suggested FIS model, the outputs, i.e., PZ extensions at the middle points of roof (1), floor (2), left sidewall (3) and right sidewall (4) along with at the key point (5) would be achieved 4.13 m, 5.55 m, 6.33 m, 10.2 m and 11.7 m, respectively. The fuzzy model results in this example also revealed that the MPZ occurred in the key point.

7 Construction of MVR model

In this research, the relationships between the output variables, i.e., PZs at different points and the input variables, i.e., geo-mechanical and geometrical parameters were established using

the MVR method. To stabilize the standard form of the MVR model and a statistical equation between the inputs and outputs variables given in Table 5, the SPSS 24 software package was applied. Accordingly, the resulted coefficients for the prediction of PZs at the middle points of roof, floor, left sidewall and right sidewall as well as at the key point were achieved in the form of Eqs. (2)–(6), respectively. As it is clear, only 7 input parameters including tensile strength, unit weight of rock, overburden depth, rock mass rating, lateral stress coefficient, crown level difference and pillar width were considered as effective parameters on PZs in statistical modeling. On the other hand, 5 input parameters including Poisson ratio, compression strength, rock mass modulus, friction angle and cohesion were deleted from the modeling. This may be due to the ineffectiveness of these parameters on the outputs in statistical approach that are automatically omitted from the modeling by software. This is the main shortage of the model and may decrease its accuracy.

Table 3 Coefficient values of Eq. (1) to predict relative PZ at the middle point of right sidewall

| <i>RMR</i> | <i>H</i> ₀ | <i>a</i> | <i>b</i> | <i>c</i> | <i>d</i> | <i>e</i> |
|------------|-----------------------|----------|------------|------------|------------|----------|
| 47 | 100 | 0.070758 | - 0.144316 | - 0.038987 | 0.021065 | 0.075526 |
| 54 | | 0.536868 | - 0.486876 | - 0.021349 | - 0.009127 | 0.101533 |
| 67 | | 1.805740 | - 0.630803 | - 0.015307 | 0.021173 | 0.050696 |
| 78 | | 1.390592 | - 0.343826 | 0.000725 | - 0.010392 | 0.018642 |
| 47 | 200 | 0.024996 | - 0.083308 | 0.054892 | - 0.052028 | 0.148007 |
| 54 | | 0.282871 | - 0.419940 | - 0.045115 | 0.002246 | 0.142862 |
| 67 | | 0.679884 | - 0.372993 | - 0.031890 | 0.089094 | 0.047996 |
| 78 | | 0.872507 | - 0.357655 | - 0.026845 | 0.033368 | 0.034914 |
| 47 | 300 | 0.026068 | - 0.162023 | - 0.158500 | - 0.128056 | 0.405257 |
| 54 | | 0.128345 | - 0.252366 | - 0.172541 | 0.194007 | 0.178925 |
| 67 | | 0.539784 | - 0.420511 | - 0.058226 | 0.126609 | 0.076158 |
| 78 | | 0.625684 | - 0.356854 | - 0.035119 | 0.088528 | 0.046514 |
| 47 | 400 | 0.014561 | - 0.117725 | - 0.213076 | - 0.132061 | 0.438055 |
| 54 | | 0.070168 | - 0.197175 | - 0.147008 | 0.307073 | 0.241251 |
| 67 | | 0.567677 | - 0.558188 | - 0.029658 | 0.173880 | 0.122001 |
| 78 | | 0.339932 | - 0.238078 | - 0.065145 | 0.122087 | 0.040565 |
| 47 | 500 | 0.008751 | - 0.086915 | - 0.240055 | - 0.296075 | 0.461544 |
| 54 | | 0.054472 | - 0.201872 | - 0.193933 | 0.337197 | 0.310596 |
| 67 | | 0.424094 | - 0.490167 | - 0.133585 | 0.093543 | 0.154652 |
| 78 | | 0.366075 | - 0.319388 | - 0.028316 | 0.151720 | 0.061611 |
| 47 | 600 | 0.006133 | - 0.071567 | - 0.574269 | - 0.559176 | 0.494960 |
| 54 | | 0.037871 | - 0.169572 | - 0.106206 | 0.186960 | 0.327149 |
| 67 | | 0.185687 | - 0.221525 | - 0.135691 | 0.523072 | 0.131913 |
| 78 | | 0.378919 | - 0.391269 | - 0.133766 | 0.276255 | 0.093717 |

Table 4 Comparison of the predicted PZs from Eq. (1) with the results of numerical program at the key point (MPZ) and middle point of the right sidewall (RS_p)

| Example | <i>K</i> | <i>h</i> (m) | <i>H</i> (m) | <i>RMR</i> | <i>B</i> (m) | <i>Z</i> (m) | Real value MPZ (m) | Predicted value MPZ (m) | Error MPZ (%) | Real value RS _p (m) | Predicted value RS _{-p} (m) | Error RS _p (%) |
|---------|----------|--------------|--------------|------------|--------------|--------------|--------------------|-------------------------|---------------|--------------------------------|--------------------------------------|---------------------------|
| 1 | 0.7 | 52 | 552 | 47 | 20 | - 10 | 20 | 19.31 | 3.4 | 14.581 | 15.6 | 7 |
| 2 | 1 | 52 | 352 | 47 | 50 | - 10 | 10.581 | 10.14 | 4.13 | 9.5 | 8.3 | 12 |
| 3 | 1.5 | 52 | 252 | 47 | 30 | 0 | 8.98 | 10.1 | 12 | 4.55 | 5.027 | 10.4 |
| 4 | 2 | 52 | 452 | 47 | 40 | 10 | 21.1 | 18.46 | 12.5 | 11.8 | 11.14 | 5 |
| 5 | 2.5 | 52 | 652 | 47 | 40 | 20 | 24.5 | 27.5 | 12 | 17.5 | 18 | 2 |
| 6 | 0.7 | 52 | 352 | 54 | 20 | - 10 | 5.955 | 6.08 | 2.2 | 3.11 | 3.14 | 1 |
| 7 | 1 | 52 | 652 | 54 | 50 | 0 | 8.862 | 8.04 | 9.1 | 6.923 | 7.69 | 11 |
| 8 | 1.5 | 52 | 452 | 54 | 30 | 0 | 8.548 | 8.17 | 4.4 | 4.68 | 4.96 | 6.1 |
| 9 | 2 | 52 | 252 | 54 | 40 | 20 | 8.49 | 8.16 | 3.8 | 2 | 1.855 | 7 |
| 10 | 2.5 | 52 | 452 | 54 | 50 | 20 | 16.3 | 16.67 | 2.17 | 12.65 | 10.96 | 13 |
| 11 | 2.5 | 52 | 252 | 67 | 40 | 0 | 5.671 | 6.42 | 13 | 2.834 | 2.55 | 9.7 |
| 12 | 0.7 | 52 | 652 | 67 | 40 | 0 | 5.725 | 5.17 | 9.5 | 3.34 | 3.32 | 0.33 |
| 13 | 2 | 52 | 352 | 67 | 40 | 20 | 5.9 | 6.2 | 4.9 | 1.389 | 1.37 | 1.5 |
| 14 | 2.5 | 52 | 552 | 78 | 30 | - 10 | 6.65 | 7.5 | 12.7 | 3.237 | 3.034 | 6.24 |
| 15 | 2.5 | 52 | 452 | 78 | 20 | 10 | 6.101 | 5.25 | 13.5 | 2.647 | 2.32 | 12 |

Table 5 Statistic descriptions and symbols of FIS and MVR modeling parameters

| Type | Variable | Sign | Maximum | Minimum | Std dev. | Var. |
|---------------------------------------|---------------------------------------|--------------------------------|---------|---------|----------|----------|
| Input | Rock unit weight (kN/m ³) | γ | 0.028 | 0.026 | 0.000824 | 6.79E-07 |
| | Tensile strength (MPa) | σ_t | 1.567 | 0.04 | 0.705 | 0.4971 |
| | Poison ratio (–) | ν | 0.27 | 0.25 | 0.01 | 0 |
| | Coefficient of lateral stress (–) | K | 2.5 | 0.7 | 0.65 | 0.43 |
| | Compression strength (MPa) | σ_c | 54.154 | 13.48 | 17.16713 | 294.7102 |
| | Rock mass modulus (GPa) | E | 40.973 | 4.35 | 15.957 | 254.62 |
| | Friction angle (°) | φ | 56.94 | 44.16 | 5.527814 | 30.55673 |
| | Cohesion (Mpa) | C | 4.976 | 1.47 | 1.6435 | 2.70111 |
| | Overburden depth (m) | H | 652 | 152 | 169.6 | 28785 |
| | Rock mass rating (–) | RMR | 78 | 47 | 13.41 | 179.9 |
| | Pillar width (m) | B | 50 | 20 | 11.2 | 124 |
| | Crown level difference (m) | Z | 20 | – 10 | 11.195 | 125.34 |
| | Output | PZ in middle point of roof (m) | I | 14.159 | 0 | 2.89061 |
| PZ in middle point of floor (m) | | II | 19.017 | 0 | 4.826364 | 23.29379 |
| PZ in left sidewall middle point (m) | | III | 21.72 | 0 | 5.2805 | 27.8737 |
| PZ in right sidewall middle point (m) | | IV | 35.01 | 0 | 5.1854 | 26.8884 |
| PZ at key point (m) | | V | 40 | 0 | 7.8028 | 60.884 |

$$I = 47.426 - 1078.207\gamma + 3.785\sigma_t + 1.884K + 0.007H - 0.392RMR - 0.0B - 0.001Z, \quad (2)$$

$$II = 62.438 - 1448.802\gamma + 4.052\sigma_t + 3.9K + 0.011H - 0.517RMR - 0.001B - 0.006Z, \quad (3)$$

$$III = 53.158 - 765.859\gamma + 6.898\sigma_t + 2.057K + 0.014H - 0.674RMR - 0.00004B - 0.005Z, \quad (4)$$

$$IV = 55.199 - 853.13\gamma + 6.675\sigma_t + 2.188K + 0.014H - 0.66RMR - 0.012B - 0.007Z, \quad (5)$$

$$V = 77.785 - 1474.688\gamma + 5.768\sigma_t + 5.325K + 0.018H - 0.771RMR - 0.062B - 0.03Z. \quad (6)$$

8 Comparative analysis

For comparing the three suggested models, their results were evaluated based on the some testing datasets that were not utilized in the construction of models. The Testing datasets were utilized for comparative analysis between the predicted PZs form the fuzzy inference system (FIS) and multivariate regression (MVR) models with the results of numerical analysis (NA). Moreover, comparative analysis was performed using the case study measurements for the verification of the three proposed models.

8.1 Comparison based on the performance index

In this section, the comparative analysis of the proposed models is conducted using some powerful performance evaluation

indices including Pearson coefficient of correlation (R), normalized of root mean square error (NRMSE), coefficient of Nash–Sutcliffe (E) and mean absolute error (MAE). The values of R and E of a model closer to 1 show the higher accuracy and better performance of it. On the contrary, the closer values of NRMSE and MAE to zero indicate the accurateness and superiority of a model. The above-mentioned performance indices are calculated as follows:

$$R = \frac{\sum_{i=1}^n (x_i - \bar{x})(y_i - \bar{y})}{\sqrt{\sum_{i=1}^n (x_i - \bar{x})^2 \sum_{i=1}^n (y_i - \bar{y})^2}}, \quad (7)$$

$$NRMSE = \frac{\sqrt{\sum_{i=1}^n (x_i - y_i)^2 / n}}{\bar{x}}, \quad (8)$$

Table 6 Some samples of datasets used in the construction of FIS and MVR models

| No. | γ (kN/m ³) | σ_1 (MPa) | ν (-) | K (-) | σ_c (MPa) | E (GPa) | ϕ (°) | C (MPa) | H (m) | RMR (-) | B (m) | Z (m) | I (m) | II (m) | III (m) | IV (m) | V (m) |
|-----|-------------------------------|------------------|-----------|---------|------------------|-----------|------------|-----------|---------|---------|---------|---------|-------|--------|---------|--------|--------|
| 1 | 0.027 | 0.04 | 0.27 | 0.7 | 13.48 | 4.35 | 44.16 | 1.47 | 352 | 47 | 40 | -10 | 1.8 | 0 | 10.543 | 10.321 | 11.121 |
| 2 | 0.027 | 0.04 | 0.27 | 1.5 | 13.48 | 4.35 | 44.16 | 1.47 | 252 | 47 | 30 | 0 | 5.169 | 8.67 | 5.026 | 4.548 | 8.948 |
| 3 | 0.027 | 0.04 | 0.27 | 2 | 13.48 | 4.35 | 44.16 | 1.47 | 452 | 47 | 50 | 20 | 8.59 | 15.2 | 10.79 | 13.75 | 15.49 |
| 4 | 0.028 | 0.145 | 0.27 | 2.5 | 25.9 | 11.9 | 54.62 | 1.6 | 152 | 54 | 20 | -10 | 1.328 | 5.16 | 3.67 | 5.5 | 17.703 |
| 5 | 0.028 | 0.145 | 0.27 | 1.5 | 25.9 | 11.9 | 54.62 | 1.6 | 552 | 54 | 40 | 10 | 3.42 | 6.17 | 5.8 | 6.04 | 8.646 |
| 6 | 0.028 | 0.145 | 0.27 | 1 | 25.9 | 11.9 | 54.62 | 1.6 | 652 | 54 | 30 | 20 | 3.3 | 5.8 | 8.6 | 8.2 | 10.628 |
| 7 | 0.026 | 0.715 | 0.25 | 1.5 | 29.97 | 29 | 51.34 | 3.09 | 452 | 67 | 50 | -10 | 2 | 4.19 | 0 | 0 | 4.415 |
| 8 | 0.026 | 0.715 | 0.25 | 2 | 29.97 | 29 | 51.34 | 3.09 | 252 | 67 | 20 | 0 | 1.735 | 2.70 | 0 | 0.614 | 3.04 |
| 9 | 0.026 | 1.567 | 0.25 | 1 | 54.15 | 40.9 | 56.94 | 4.976 | 352 | 78 | 40 | 10 | 0 | 0 | 0 | 0 | 0 |
| 10 | 0.026 | 1.567 | 0.25 | 2.5 | 54.15 | 40.9 | 56.94 | 4.976 | 652 | 78 | 30 | 20 | 1.57 | 6.3 | 5.062 | 4.701 | 7.2 |

$$E = 1 - \frac{\sum_{i=1}^n (x_i - y_i)^2}{\sqrt{\sum_{i=1}^n (x_i - \bar{x})^2}}, \tag{9}$$

$$MAE = \frac{\sum_{i=1}^n |(x_i - y_i)|}{n}, \tag{10}$$

where x_i is the i th observation (measured) value, y_i is the i th estimated element (model output), \bar{x} and \bar{y} are the average values of the measured and predicted data, respectively, and; n indicates the datasets number.

Based on the testing data series, the above-mentioned indices were calculated for FIS and MVR models and for the Eq. (1) obtained from NM. The acquired results from these calculations are summarized in Table 7. As shown, the R and E values for FIS and NM are significantly greater than those values for MVR model which indicates the high accuracy of FIS and NM models. On the other hand, NRMSE and MAE values of these models are considerably lower than those of the MVR model. According to this comparative task, it is understood that the suggested FIS model and NM-based equation (Eq. (1)) can be successfully applied in estimating PZs around the power station caverns with better efficiency compared to the MVR model. However, some of the effective input variables were automatically deleted in the MVR modeling that decreases its capability and reliability in the estimation of PZs unlike the FIS and NM modeling.

8.2 Comparison based on the simulation results

For more assessment of the suggested models, comparative analysis is conducted in this section based on their simulation results in the form of determination coefficient (R^2). Relationship between the predicted PZs achieved from the FIS, NM and MVR models with the NA results is depicted in Figs. 7, 8, 9, respectively. These comparisons were conducted using the testing data series that were not utilized in the suggested models construction. It can be concluded from these figures that resulted R^2 from the suggested FIS and NM models are higher than the results of MVR approach. The high resulted values of R^2 from the FIS and NM models indicate the high capability of these models in the estimation of PZs around the power station caverns. However, the proposed MVR model could be also applied to situations in which relative approximation of PZs would be sufficient.

8.3 Comparison based on the case study measurements

In this section, measured parameters of some underground opening case studies, collected from the valid literatures, are used as a basis for models comparison and verification.

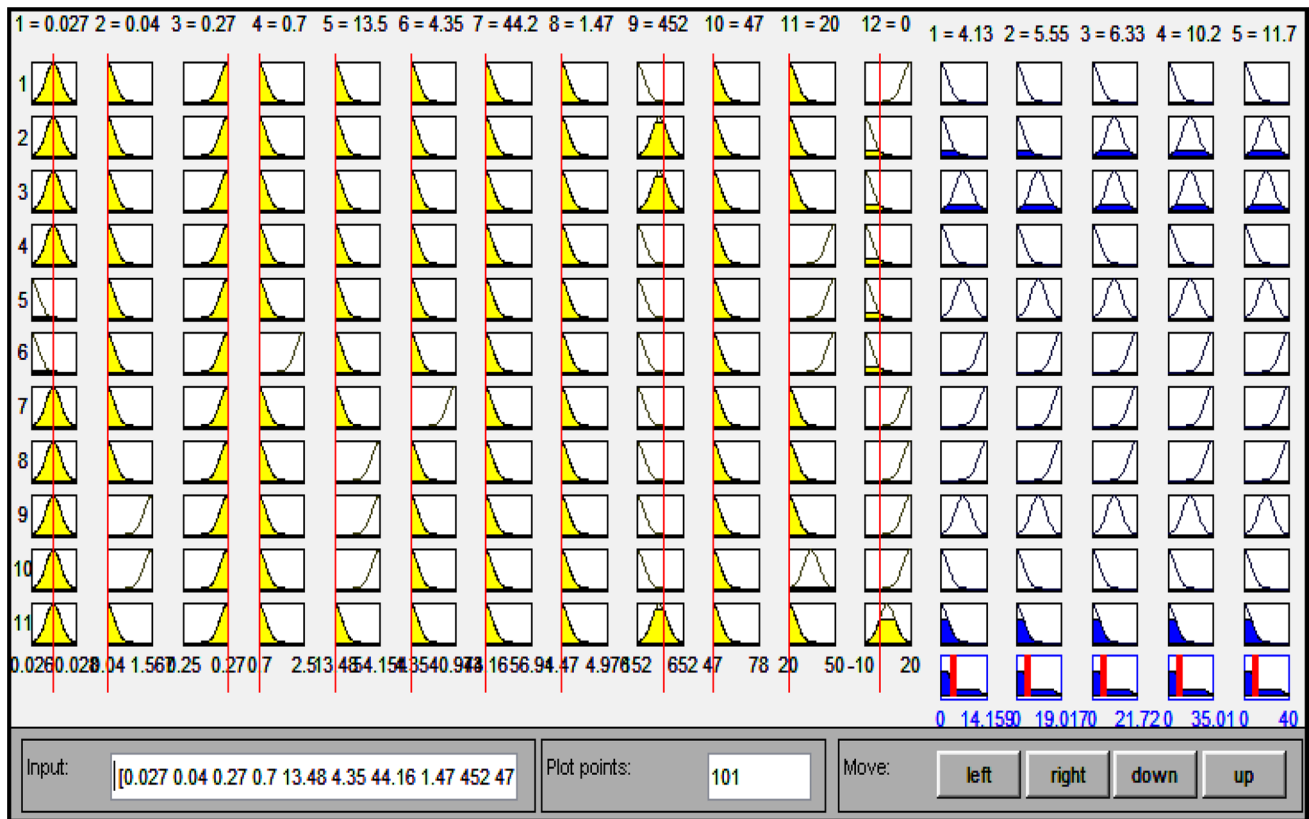


Fig. 6 Schematic representation example of suggested FIS aggregation process

Table 7 Computed statistical indices for the proposed models in PZs prediction

| Index Model | | R | NRMSE | E | MAE |
|-------------------------------|-----------------------|--------|-------|-------|------|
| FIS | PZ in roof | 0.9904 | 0.024 | 0.981 | 0.43 |
| | PZ in floor | 0.9871 | 0.031 | 0.965 | 0.61 |
| | PZ in left side-wall | 0.995 | 0.022 | 0.987 | 0.34 |
| | PZ in right side-wall | 0.9841 | 0.033 | 0.956 | 0.79 |
| | PZ in key point | 0.997 | 0.012 | 0.984 | 0.28 |
| MVR | PZ in roof | 0.9009 | 0.063 | 0.858 | 1.02 |
| | PZ in floor | 0.9095 | 0.101 | 0.862 | 1.92 |
| | PZ in left side-wall | 0.8722 | 0.128 | 0.81 | 2.35 |
| | PZ in right side-wall | 0.8977 | 0.125 | 0.833 | 2.27 |
| | PZ in key point | 0.8868 | 0.182 | 0.827 | 3.12 |
| Equation (1) obtained from NM | PZ in roof | – | – | – | – |
| | PZ in floor | – | – | – | – |
| | PZ in left side-wall | – | – | – | – |
| | PZ in right side-wall | 0.992 | 0.011 | 0.975 | 0.22 |
| | PZ in key point | 0.998 | 0.007 | 0.989 | 0.13 |

Measured properties along with the actual values of MPZ (value of PZ in key point) are demonstrated in Table 8. As an evaluation criterion, the MPZ resulted from the proposed models for the mentioned case studies (given in Table 8) are compared with the actual MPZ. Results of this comparison along with the resulted errors of the proposed models are shown in Table 9. It is obvious from this comparison that the results of NA and FIS proposed models are in accordance with the actual MPZ values and have the acceptable errors. This proved the capability of the proposed approaches in this research, i.e., NA and FIS models and their abroad applications unlike the previous available models in this field.

9 Parametric study

In modeling processes, parametric study or sensitivity analysis is commonly conducted to assess the impact of model input/autonomous parameters on its object/output parameter(s). For this purpose, the virtual influence of an input/autonomous parameter on the corresponding object/output(s) was achieved by varying the intended input parameter and considering the fixed values for the other variables [47–49]. Besides, the available common methods of sensitivity analysis can be utilized. In the current paper, parametric

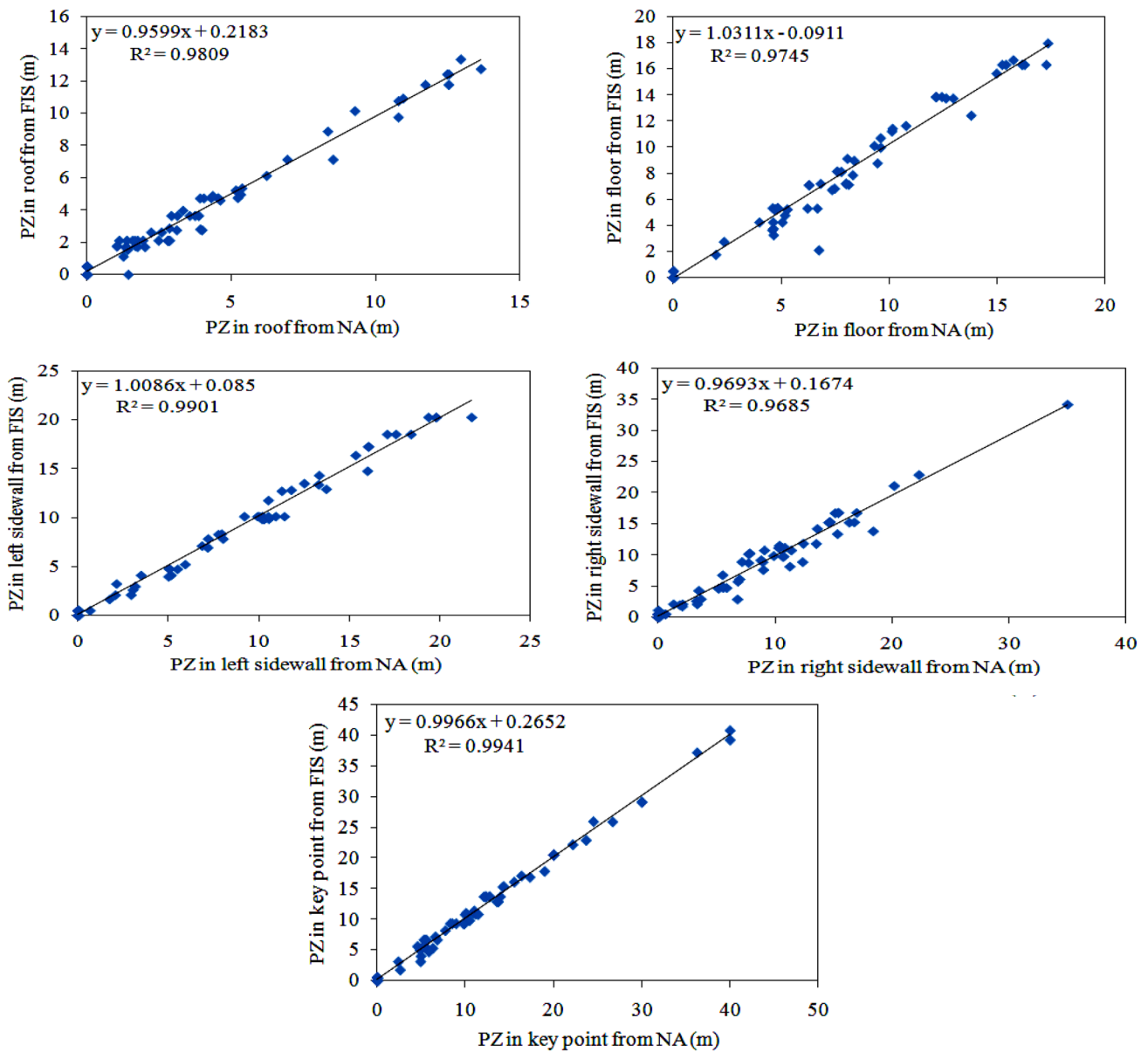


Fig. 7 Relationship of actual values and predicted PZs from the FIS model

study was conducted based on the method of cosine amplitude which is the most used sensitivity analysis approach in the engineering fields [50–57]. The following equation is generally applied to calculate the weight of the input/autonomous variables (r_{ij}) on the object/output(s) in this sensitivity analysis method.

$$r_{ij} = \frac{\sum_{k=1}^m x_{ik}x_{jk}}{\sqrt{\sum_{k=1}^m x_{ik}^2 \sum_{k=1}^m x_{jk}^2}} \quad (11)$$

In the above equation, x_{ik} is the k th input/autonomous parameter and x_{jk} is the corresponded k th model object/output of those input value.

Here, the influences of input variables on PZs around the power station cavern in the FIS model were calculated using the Eq. (11). The results of FIS model sensitivity analysis for determining PZ in different points around the powerhouse are graphically demonstrated in Fig. 10. According to this figure, lateral stress coefficient, rock mass modulus, overburden depth, lateral stress coefficient and rock mass rating are the most effective parameters on PZ at the middle points of roof, floor, left sidewall and right sidewall, and at the key point, respectively. In contrast, the tensile strength

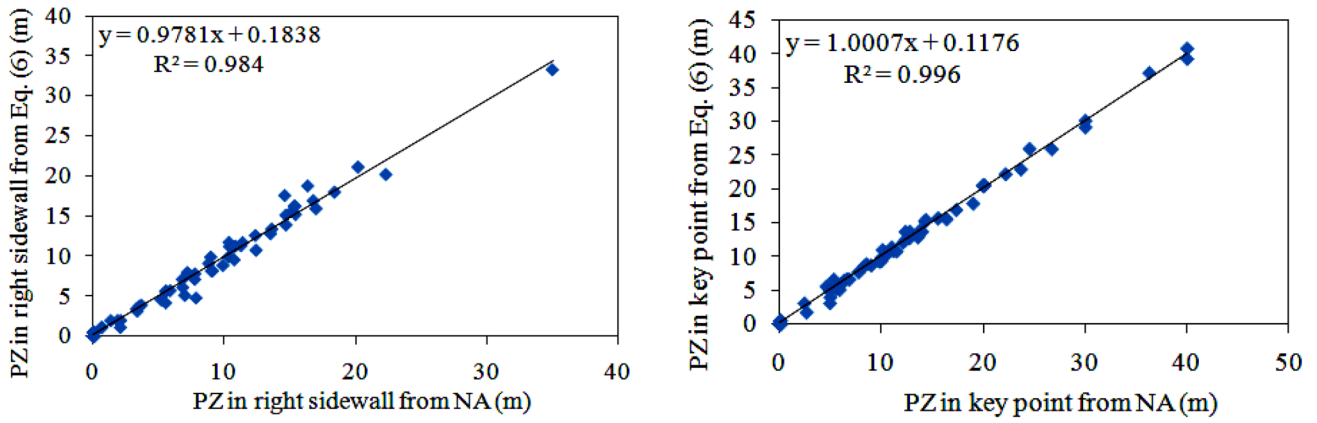


Fig. 8 Relationship of actual values and predicted PZs from the NM model (Eq. (1))

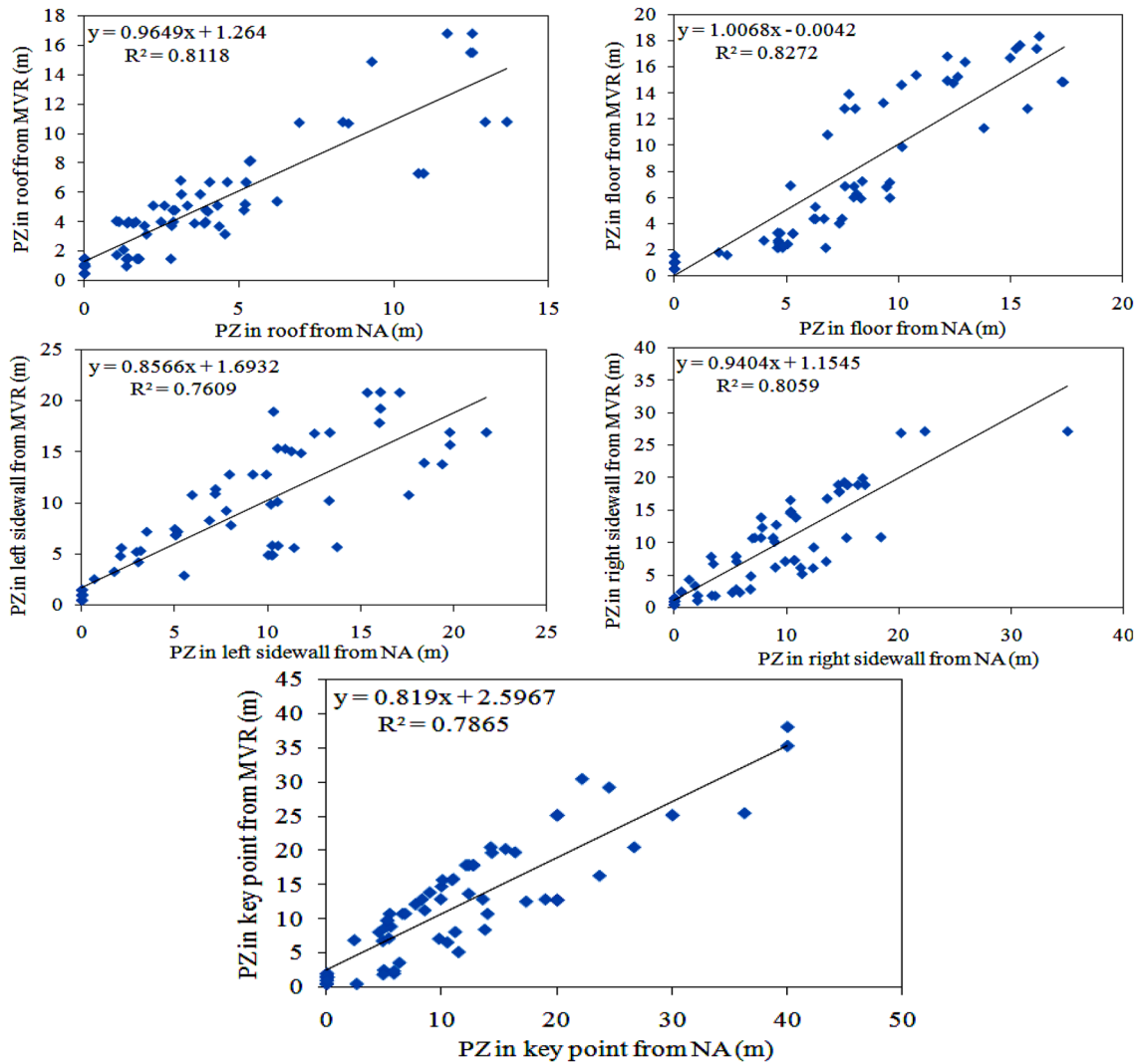


Fig. 9 Relationship of actual values and predicted PZs from the MVR model

Table 8 Measured properties of some case studies along with the actual values of MPZ

| Case no. | Parameters | | | | | | | | | | | References | | |
|----------|------------|--------------|-------------------------------|--------------|----------------|----------------|------------|------------------|-----|--------------|--------------|------------|---------|---|
| | <i>K</i> | <i>h</i> (m) | γ (KN/m ³) | <i>H</i> (m) | <i>E</i> (Gpa) | <i>C</i> (MPa) | ϕ (°) | σ_c (MPa) | RMR | <i>B</i> (m) | <i>Z</i> (m) | | MPZ (m) | Error (%) |
| 1 | 1 | 9 | 23 | 130 | 0.958 | 0.471 | 38.12 | – | 45 | 0 | 0 | 5.173 | 12.3 | Abdollahipour and Rahmamejad [41] |
| 2 | 3.1 | 24 | 26.20 | 80 | 3.7 | 1.8 | 52.1 | 11.4 | 47 | 38 | 0 | 2.75 | 2.5 | Liu et al. [42] |
| 3 | 1 | 34.55 | 25.5 | 249.6 | 1.5 | 0.65 | 30 | – | 45 | 35.7 | 27.75 | 6.85 | 14.16 | Sopaci and Akgün [43] |
| 4 | 1.5 | 46 | 26 | 346 | 6 | 1 | 50 | – | 49 | 29 | –8 | 9.3 | 15.1 | Sinotech Engineering Consultants Inc [44] |
| 5 | 1.31 | 7 | 26.5 | 507 | 0.876 | 0.67 | 20.59 | 1.46 | 45 | 0 | 0 | 25.01 | 0.8 | Hosseinitoudeshki [45] |
| 6 | 0.8 | 8 | 27.2 | 400 | 7.089 | 3.5 | 27 | 14.54 | 52 | 0 | 0 | 3.31 | 10 | Panda [46] |

was defined as the least effective parameter on PZ at all of the above-mentioned points.

10 Conclusions

Estimation of PZ around the power station caverns at different points including middle points of roof, floor, left sidewall and right sidewall along with the key points was studied in this research. For this purpose, two new methodologies including NA and FIS models along with the MVR analysis were proposed. The following key conclusions can also be drawn:

- On the basis of the numerical analysis outputs, an optimum empirical equation was extracted to determine PZs at the middle point of powerhouse sidewall and its key point.
- The FIS and MVR models were constructed based on the numerous data series resulted from the numerical experiments.
- To evaluate the proposed models, statistical assessment indices including *R*, *E*, *E_a*, *E_r* and NRMSE were utilized. Comparison results proved the higher validity of the NA and FIS models compared to the MVR. However, the MVR model can be applied to situations in which the relative approximation would be satisfied.
- Parametric study was conducted to assess the impact of input variables on the outputs. Accordingly, it was found that lateral stress coefficient, rock mass modulus, overburden depth, lateral stress coefficient and rock mass rating are the most effective variables on PZ at roof, floor, left sidewall, right sidewall and key point, respectively. However, tensile strength was proved as a least effective variable on the output at all the above-mentioned five points.
- Considering the above results, it can be concluded that three main findings were achieved from this research. Firstly, a verified numerical-based equation was developed for PZ estimation at the key points and middle point of the powerhouse right sidewalls. Secondly, a powerful worldwide FIS model was developed to predict the plastic zones around the caverns. Finally, plastic zones at roof, floor and side walls along with the key point or maximum plastic zone can be simultaneously estimated from this research outputs. This helps in obtaining the comprehensive knowledge of the cavern environments and precise designing of its related support systems.

Table 9 Results of the proposed models for the understudied case studies

| Case no. | Actual MPZ (m) | Models predicted MPZ (m) | | | Error of the models (%) | | |
|----------|----------------|--------------------------|-------|------|-------------------------|-------|-------|
| | | NA | FIS | MVR | NA | FIS | MVR |
| 1 | 2.75 | 2.68 | 2.66 | 1.98 | 2.5 | 3.27 | 27.74 |
| 2 | 5.173 | 4.533 | 4.52 | 1.68 | 12.3 | 12.6 | 67.45 |
| 3 | 6.85 | 7.80 | 7.84 | 1.35 | 14.16 | 14.45 | 80.22 |
| 4 | 9.3 | 10.7 | 10.71 | 1.53 | 15.1 | 15.16 | 83.47 |
| 5 | 25.01 | 24.8 | 24.6 | 2.01 | 0.8 | 1.63 | 91.95 |
| 6 | 3.31 | 2.97 | 2.96 | 1.08 | 10 | 10.57 | 67.24 |

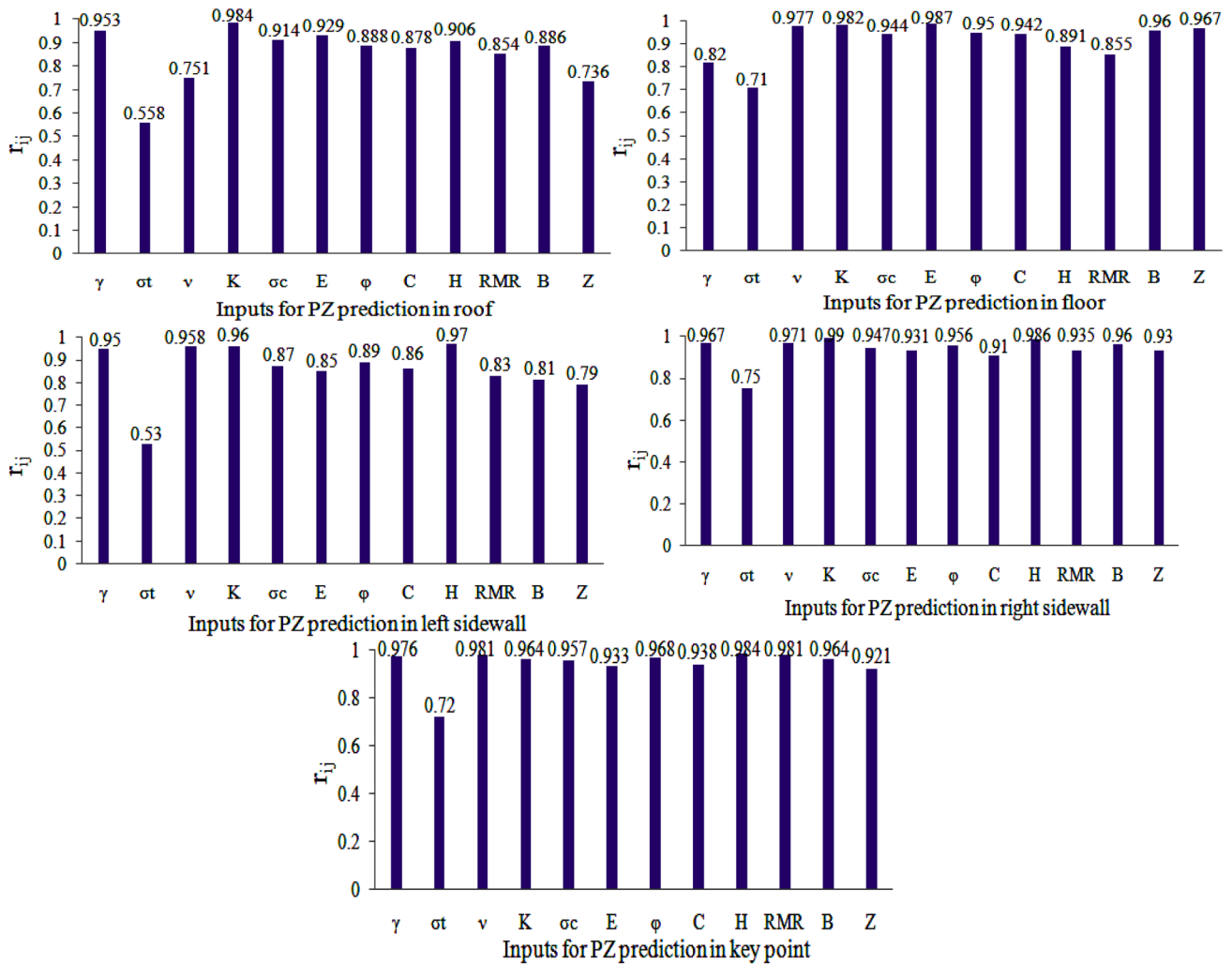


Fig. 10 Influence values of input variables on PZ at different points around the powerhouse cavern

Compliance with ethical standards

Conflict of interest All of the authors have declared that no conflict of interest is encompassed for the current research.

References

- Zhu WS, Sui B, Li XJ, Li SC, Wang WT (2008) A methodology for studying the high wall displacement of large scale underground cavern complexes and it's applications. *Tunn Undergr Sp Technol* 23(6):651–664

2. Chong L, Jinhai X, Jianzhong P, Chao M (2012) Plastic zone distribution laws and its types of surrounding rock in large-span roadway. *Int J Min Sci Technol* 22(1):23–28
3. Feng W, Huang R, Li T (2012) Deformation analysis of a soft-hard rock contact zone surrounding a tunnel. *Tunn Undergr Sp Technol* 32:190–197
4. Xiang Y, Feng S (2013) Theoretical prediction of the potential plastic zone of shallow tunneling in vicinity of pile foundation in soils. *Tunn Undergr Sp Technol* 38:115–121
5. Zhang W, Goh ATC (2014) Multivariate adaptive regression splines model for reliability assessment of serviceability limit state of twin caverns. *Geomech Eng* 7(4):431–458
6. Chen YF, Zheng HK, Wang M, Hong JM, Zhou CB (2015) Excavation-induced relaxation effects and hydraulic conductivity variations in the surrounding rocks of a large-scale underground powerhouse cavern system. *Tunn Undergr Sp Technol* 49:253–267
7. Yu S, Zhu WS, Yang WM, Zhang DF, Ma QS (2015) Rock Bridge fracture model and stability analysis of surrounding rock in underground cavern group. *Struct Eng Mech* 53(3):481–495
8. Zhang W, Goh ATC (2016) Predictive models of ultimate and serviceability performances for underground twin caverns. *Geomech Eng* 10(2):175–188
9. Zhang QB, He L, Zhu WS (2016) Displacement measurement techniques and numerical verification in 3D geomechanical model tests of an underground cavern group. *Tunn Undergr Sp Technol* 56:54–64
10. Li HB, Yang XG, Zhang XB, Zhou JW (2017) Deformation and failure analyses of large underground caverns during construction of the Houziyan Hydropower Station, Southwest China. *Eng Fail Anal* 80:164–185
11. Jiang Q, Su G, Feng XT, Chen G, Zhang MZ, Liu C (2018) Excavation optimization and stability analysis for large underground caverns under high geostress: a case study of the Chinese Laxiwa project. *Rock Mech Rock Eng* 52(3):1–21
12. Behnia M, Cheraghi Seifabad M (2018) Stability analysis and optimization of the support system of an underground powerhouse cavern considering rock mass variability. *Environ Earth Sci* 77:645. <https://doi.org/10.1007/s12665-018-7835-2>
13. Gao X, Chuan Yan E, Jim Yeh TC, Cai JS, Liang Y, Wang M (2018) A geostatistical inverse approach to characterize the spatial distribution of deformability and shear strength of rock mass around an unlined rock cavern. *Eng Geol* 245(1):106–119
14. Li X, Chen HM, Sun Y, Zhou R, Wang L (2018) Study on the splitting failure of the surrounding rock of underground caverns. *Geomech Eng* 14(5):499–507
15. Xua MF, Wu SC, Gao YT, Ma J, Wu QL (2019) Analytical elastic stress solution and plastic zone estimation for a pressure relief circular tunnel using complex variable methods. *Tunn Undergr Sp Technol* 84:381–398
16. Wang M, Li HB, Han JQ, Xiao XH, Zhou JW (2019) Large deformation evolution and failure mechanism analysis of the multi-freeface surrounding rock mass in the Baihetan underground powerhouse. *Eng Fail Anal* 100:214–226
17. Ren Q, Xu L, Zhu A, Shan M, Zhang L, Gu J, Shen L (2019) Comprehensive safety evaluation method of surrounding rock during underground cavern construction. *Undergr Sp*. <https://doi.org/10.1016/j.undsp.2019.10.003>
18. Li B, Xu N, Dai F, Zhang G, Xiao P (2019) Dynamic analysis of rock mass deformation in large underground caverns considering microseismic data. *Int J Rock Mech Min Sci* 122:104078. <https://doi.org/10.1016/j.ijrmm.2019.104078>
19. Monjezi M, Rezaei M, Yazdyan Varjani A (2009) Prediction of rock fragmentation due to blasting in Gol-E-Gohar iron mine using fuzzy logic. *Int J Rock Mech Min Sci* 46(8):1273–1280
20. Monjezi M, Rezaei M, Yazdyan A (2010) Prediction of back-break in open-pit blasting using fuzzy set theory. *Expert Syst Appl* 37(3):2637–2643
21. Monjezi M, Rezaei M (2011) Developing a new fuzzy model to predict burden from rock geomechanical properties. *Expert Syst Appl* 38(3):9266–9273
22. Rezaei M, Yazdyan Monjezi M, Varjani A (2011) Development of a fuzzy model to predict flyrock in surface mining. *Saf Sci* 49(2):298–305
23. Rezaei M, Majdi A, Monjezi M (2014) An intelligent approach to predict unconfined compressive strength of rock surrounding access tunnels in longwall coal mining. *Neural Comput Appl* 24(1):233–241
24. Rezaei M, Asadizadeh M, Hossaini MF, Majdi A (2015) Prediction of representative deformation modulus of longwall panel roof rock strata using Mamdani fuzzy system. *Int J Min Sci Technol* 25(1):23–30
25. Rezaei M (2018) Indirect measurement of the elastic modulus of intact rocks using the Mamdani fuzzy inference system. *Measurement* 129:319–331
26. Rezaei M (2019) Forecasting the stress concentration coefficient around the mined panel using soft computing methodology. *Eng Comput* 35(2):451–466
27. Liu C, Gu C, Chen B (2017) Zoned elasticity modulus inversion analysis method of a high arch dam based on unconstrained lagrange support vector regression (support vector regression arch dam). *Eng Comput* 33(3):443–456
28. Shirani Faradonbeh R, Taheri A (2019) Long-term prediction of rockburst hazard in deep underground openings using three robust data mining techniques. *Eng Comput* 35(2):659–675
29. Ghasemi E, Gholizadeh H, Adoko AC (2019) Evaluation of rockburst occurrence and intensity in underground structures using decision tree approach. *Eng Comput*. <https://doi.org/10.1007/s00366-018-00695-9>
30. Rezaei M, Asadizadeh M (2019) Predicting unconfined compressive strength of intact rock using new hybrid intelligent models. *J Min Environ*. <https://doi.org/10.22044/jme.2019.8839.1774>
31. Liao CP (1993) Fuzzy influence function method for calculating mine subsidence in a horizontal seam. *Geotech Geol Eng* 11(4):235–247
32. Li W, Mei S, Zai S, Zhao S, Liang X (2006) Fuzzy models for analysis of rock mass displacements due to underground mining in mountainous areas. *Int J Rock Mech Min Sci* 43(4):503–511
33. Rezaei M, Rajabi M (2018) Vertical displacement estimation in roof and floor of an underground powerhouse cavern. *Eng Fail Anal* 90:290–309
34. Jing L (2003) A review of techniques advances and outstanding issues in numerical modelling for rock mechanics and rock engineering. *Int J Rock Mech Min Sci* 40(3):283–353
35. Zadeh LA (1965) Fuzzy sets. *Inf Control* 8(3):338–353
36. Mamdani EH, Assilian S (1975) An experiment in linguistic synthesis with a fuzzy logic controller. *Int J Man Mach Stud* 7(1):1–13
37. Liitiainen E, Verleysen M, Corona F, Lendasse A (2009) Residual variance estimation in machine learning. *Neurocomputing* 72(16–18):3692–3703
38. Hoek E, Carranza-Torres C, Corkum B (2002) Hoek–Brown failure criterion 2002 edition. In: *Proceedings of the 5th North American Rock Mechanics Symposium, Toronto, July*, pp 267–273
39. Rajabi M, Rahmnejad R, Rezaei M, Ganjalipour K (2017) Evaluation of the maximum horizontal displacement around the power station caverns using artificial neural network. *Tunn Undergr Sp Technol* 64:51–60
40. Zhu WS, Li XJ, Zhang QB, Zheng WH, Xin XL, Sun AH, Li SC (2010) A study on sidewall displacement prediction and stability

- evaluations for large underground power station caverns. *Int J Rock Mech Min Sci* 47(7):1055–1062
41. Abdollahipour A, Rahmamejad R (2013) Investigating the effects of lateral stress to vertical stress ratios and caverns shape on the cavern stability and sidewall displacements. *Arabian J Geosci* 6(12):4811–4819
 42. Liu J, Zhao XD, Zhang SJ, Xie LK (2018) Analysis of support requirements for underground water-sealed oil storage cavern in China. *Tunn Undergr Sp Technol* 71:36–46
 43. Sopacı E, Akgün H (2008) Engineering geological investigations and the preliminary support design for the proposed Ordu Peripheral Highway Tunnel, Ordu, Turkey. *Eng Geol* 96(1–2):43–61
 44. Sinotech Engineering Consultants Inc (1999) Design of large underground caverns—a case history based on the Mingtan Pumped Storage Project in Taiwan. *Geotech Geol Eng* 23:175–197
 45. Hosseinitoudeshki V (2013) Numerical analysis of K0 to tunnels in rock masses exhibiting strain-softening behaviour (case study in Sardasht dam tunnel, NW Iran). *Int Res J Basic Appl Sci* 4(6):1572–1581
 46. Panda MK, Mohanty S, Pingua BMP, Mishra AK (2014) Engineering geological and geotechnical investigations along the head race tunnel in Teesta Stage-III hydroelectric project, India. *Eng Geol* 181(1):297–308
 47. Rezaei M, Hossaini MF, Majdi A (2015) Development of a time-dependent energy model to calculate the mining-induced stress over gates and pillars. *J Rock Mech Geotech Eng* 7(3):306–317
 48. Rezaei M (2018) Long-term stability analysis of goaf area in longwall mining using minimum potential energy theory. *J Min Environ* 9(1):169–182
 49. Rezaei M, Farouq Hossaini M, Majdi A, Najmoddini I (2018) Study the roof behavior over the longwall gob in long-term condition. *J Geol Min Res* 10(2):15–27
 50. Khoshjavan S, Mazlumi M, Rezai B, Rezai M (2010) Estimation of hardgrove grindability index (HGI) based on the coal chemical properties using artificial neural networks. *Orient J Chem* 26(4):1271–1280
 51. Sayadi AR, Tavassoli SMM, Monjezi M, Rezaei M (2014) Application of neural networks to predict net present value in mining projects. *Arabian J Geosci* 7(3):1067–1072
 52. Majdi A, Rezaei M (2013) Application of artificial neural networks for predicting the height of destressed zone above the mined panel in longwall coal mining. In: 47th U.S. Rock Mechanics/ Geomechanics Symposium, San Francisco, June, pp 1665–1673
 53. Rezaei M, Hossaini MF, Majdi A, Najmoddini I (2017) Determination of the height of destressed zone above the mined panel: an ANN model. *Int J Min Geo-Eng* 51(1):1–7
 54. Rezaei M (2017) Feasibility of novel techniques to predict the elastic modulus of rocks based on the laboratory data. *Int J Geotech Eng*. <https://doi.org/10.1080/19386362.2017.1397873>
 55. Rezaei M (2018) Development of an intelligent model to estimate the height of caving–fracturing zone over the longwall gobs. *Neural Comput Appl* 30(7):2145–2158
 56. Nikafshan Rad H, Hasanipanah M, Rezaei M, Lotfi Eghlim A (2018) Developing a least squares support vector machine for estimating the blast-induced flyrock. *Eng Comput* 34(4):709–717
 57. Asadzadeh M, Rezaei M (2019) Surveying the mechanical response of nonpersistent jointed slabs subjected to compressive axial loading utilising GEP approach. *Int J Geotech Eng*. <https://doi.org/10.1080/19386362.2019.1596610>

Publisher's Note Springer Nature remains neutral with regard to jurisdictional claims in published maps and institutional affiliations.